Time lens for high-resolution neutron time-of-flight spectrometers

K. Baumann

Technische Universität, D-80333 München, Germany

R. Gähler, P. Grigoriev,* and E. I. Kats*

Institut Laue Langevin, F-38042 Grenoble, France
(Received 7 July 2005; published 28 October 2005)

We examine in analytic and numeric ways the imaging effects of temporal neutron lenses created by traveling magnetic fields. For fields of parabolic shape we derive the imaging equations, investigate the time magnification, the evolution of the phase-space element, the gain factor, and the effect of finite beam size. The main aberration effects are calculated numerically. The system is technologically feasible and should convert neutron time-of-flight instruments from pinhole to imaging configuration in time, thus enhancing intensity and/or time resolution. Further fields of application for high-resolution spectrometry may be opened.

I. INTRODUCTION

A standard lens will image all points $\mathbf{r}_0$ from the object plane to all points $\mathbf{r}_d$ in the image plane, and all rays emerging from $\mathbf{r}_0$ within a certain aperture will arrive at $\mathbf{r}_d$ no matter what their initial propagation direction was. For optics in time one should form the image of an initial event at $t=0, \mathbf{r}_0$, at a final event $t_d, \mathbf{r}_d$, and to have an ideal time-dependent optical device, all rays leaving the initial event, whatever their initial velocities are, will arrive at the final event.

Intensive work on electromagnetic imaging in time started in the late 1960s by the development of chirp radar, where pulse compression—imaging in time—in a dispersive medium is achieved by proper frequency modulation of quadratic shape around the center of a traveling wave. Here we only refer to the beautiful review article on temporal imaging by Kolner [1], who fully worked out the space-time duality in imaging, based on the relations between the Helmholtz equation for paraxial imaging and narrowband dispersion. Time microscopes and telescopes are introduced as well in this paper. More recent work deals with time-dependent dielectrics in interferometry [2].

In atom optics, time lenses have been proposed and realized. The rather low matter-wave frequencies of ultracold atoms can be shifted by high-frequency modulated light, such that matter-wave dispersion in free space leads to temporal imaging. Here we refer to a paper by Arnd *et al.* [3] who observed temporal imaging of atoms via a light mirror, modulated by a time function which resembles the spatial function of a Fresnel lens used for spatial imaging. A time lens for atoms based on a magnetic field of parabolic shape and very short pulse width was realized by E. Maréchal *et al.* [4]. Time interferometry was realized for cold atoms [5], in shifting their matter-wave frequencies by time-modulated light waves.

Longitudinal compression of electron beams to enhance the performance of free-electron lasers has found strong theoretical interest (see for example [6]).

For neutrons, optics in time was stimulated by early papers [7,8], calculating the interaction of a plane wave with an aperture, which opens suddenly in time. Imaging in time was achieved by high-frequency mechanical chopping of the amplitude of ultracold neutrons [9,10]. The slit pattern on the chopper resembled a one-dimensional Fresnel zone plate, so the modulation frequency changed quadratically with the time distance from the "optical time axis." Theoretical work on these subjects [11] and also on time interferometry [12] has been published. Closely related phenomena, like diffraction from vibrating surfaces [13], diffraction from time-dependent slits [14], and interferences induced by time-dependent B fields [15] have been observed as well.

Following the techniques known in charged-particle accelerator physics, a neutron lens can also be created by electromagnetic forces traveling with the particle beam. Instead of the mainly electrical forces providing acceleration of charged particles, the gradient of a magnetic field can be the driving force of a neutron, possessing a magnetic moment. In agreement with Liouville's theorem the phase-space volume is conserved but the neutrons can be concentrated into certain intervals. These ideas were first discussed by Rauch and co-workers [16,17], who studied moving magnetic fields with parabolic shape in the direction of neutron propagation. Their aim was to tailor neutron beams supplied by future pulsed neutron sources. Beam monochromatization, i.e., temporal imaging to infinity, bunching, and cooling of polarized neutron beams were discussed and these methods may advance neutron spectroscopy.

Our proposal is closely related to their idea, but we follow a different approach and the realization in our case looks less challenging. We want to replace the pinholelike time optics of neutron time-of-flight (TOF) spectrometers by an imaging system based on a traveling magnetic field. The idea can best be seen from Fig. 1.

In the standard pinhole case, the time width of the pulse at the detector is a convolution of both chopper openings. In the imaging case the entrance slit, which may have a rather small

---

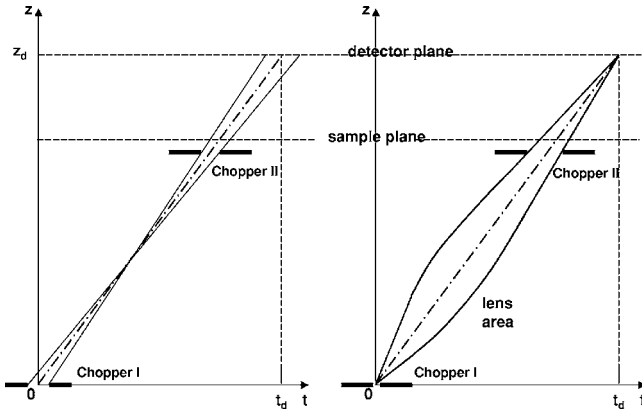*Also at L.D. Landau Institute for Theoretical Physics, RAS, Moscow, Russia.

043619-1

FIG. 1. Space-time diagrams of a standard TOF spectrometer (left) and an imaging TOF spectrometer (right). In the standard case, the second chopper acts as a pinhole camera in time, imaging the first chopper opening time. In the right case, the second chopper merely acts as an aperture for the time lens.
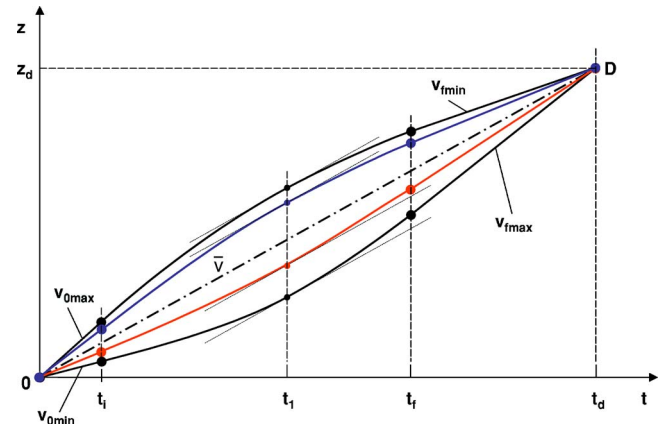

FIG. 2. (Color online) Space-time diagram for time imaging. The origin ($z=0, t=0$) is imaged to a point ($z=z_d, t=t_d$) via a time lens, whose action is switched on at t_i and terminated at t_f. At the principal time t_1 all velocities are equal.

time width, is imaged in time onto the plane of detection and the second slit plays merely the role of the lens aperture, limiting the effect of lens aberrations and limiting the spectral width of the pulse. The imaging system should enhance the intensity and/or the time resolution for time-of-flight spectrometers and open additional beam-handling capabilities.

Those instruments gather important insights in numerous domains of present solid state research, as in the dynamics of high-T_c superconductors [18,19], in the change of dynamics upon crystal-glass transitions [20], or in the spin Hamiltonians of magnetic clusters [21]. A high-resolution cold-neutron TOF spectrometer—the type we aim to improve—was one of the first instruments, being formally approved at the SNS in Oakridge.

The remainder of our paper has the following structure. The next section contains all basic methodical details and equations necessary for our investigation. Many of the points made below can be found in the literature but to our knowledge they have never been concisely written down aiming at proposing and studying a time lens for neutron TOF spectrometers. Armed with this knowledge we then discuss possible design parameters and miscellaneous subjects related to time-lens focusing. We close with numerical calculations for a time lens with realistic parameters.

II. CALCULATION OF THE MAGNETIC FIELD PROFILE

We want to focus a neutron beam in time, emitted at point $O, t=0, z=0$, to point $D, t=t_d, z=z_d$ [see the time-coordinate ($t-z$) diagram Fig. 2], assuming a paraxial beam along $0 \leqslant z \leqslant z_d$. For this purpose we need to apply some external force $F(t,z)$ to the neutrons. This force is turned on at time $t_i > 0$ and is turned off at time $t_f > t_i$. Before t_i or after t_f the neutrons move with constant velocities. To find the required force $F(t,z)$ we assume that the time interval of emission around $t=0$ is much less than the time t_i. Then the trajectories of neutrons do not intersect and are determined only by the initial velocities of neutrons v_0, shown as different slopes

in the z-t diagram. The neutron coordinates at time t_i, when F is turned on, are given by

$$z_i = v_0 t_i. \tag{1}$$

It is possible to focus the neutrons to the common point D keeping the trajectories nonintersected. At the time t_f, when F is turned off, each neutron must have a velocity v_f related to its coordinate z_f given by the equation

$$v_f = (z_d - z_f)/(t_d - t_f). \tag{2}$$

In this case all neutrons will meet at D, the space-time focal point of the system.

The force $F(z,t)$ determines the neutron acceleration $a(z,t) \equiv F(z,t)/m_n$, where m_n is the neutron mass. We will look for a special solution $a(z,t)$, where for each neutron j the acceleration will be constant during the full time range from t_i to t_f. For each neutron the acceleration is only determined by its initial and final velocities via

$$a_j = (v_f - v_0)/(t_f - t_i). \tag{3}$$

With this choice, the acceleration of each neutron is constant in time but depends on the initial velocity.

The above conditions, together with the nonintersection of all trajectories $z(v,t)$ and the constant acceleration between t_i and t_f for each neutron, imply a velocity-time diagram as shown in Fig. 3, where at a certain time t_1 all velocities v have the same values $v = \bar{v} = z_d/t_d$. Note that for all trajectories (some are shown in Fig. 3) the shaded areas left and right from t_1 must be equal, as

$$z_d = \int_0^{t_d} v(t)dt \tag{4}$$

is equal for all neutrons. In analogy to optics in space, t_1 is called the principal time of the system. From Fig. 3 and Eq. (4) we get
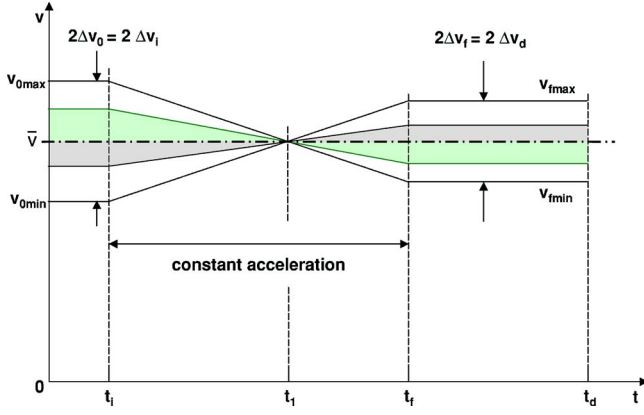
FIG. 3. (Color online) The integrals (shaded areas) for each individual particle velocity left and right from the principal time t_1 must be equal in order to satisfy the imaging conditions.

$$t_1 \equiv t_f - \frac{t_f^2 - t_i^2}{2t_d}. \tag{5}$$

Imaging to infinity in time ($t_d \to \infty$) requires $t_1 = t_f$, i.e., the lens action is terminated at the principal time, when all neutrons have the same velocity.

The velocity-time diagram Fig. 3 also shows that the velocity bandwidth changes from $2\Delta v_0$ at t_i to $2\Delta v_d$ at t_d with

$$\Delta v_0 / \Delta v_d = (t_1 - t_i)/(t_f - t_1). \tag{6}$$

The evolution of a small rectangular phase-space element with time upon the passage of the pulse through the optics (obtained analytically and then checked by the Monte Carlo calculation) is presented in Fig. 4. It shows (for details see Sec. IV) that for small enough values of Δv_0 and Δz_0 a rectangular phase-space element at t_0 transforms to a parallelogram (near-rectangular) phase-space element at t_d. Due to Liouville's theorem the phase-space volume of the neutron
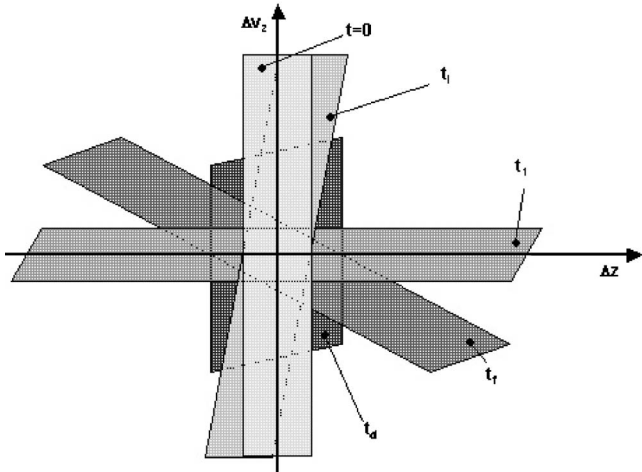

FIG. 4. The evolution of the phase-space element with time ($t = 0 \to t_i \to t_1 \to t_f \to t_d$) calculated from the evolution of its four corner points. From this picture, a simple formula for the time magnification M is obtained: $M = \Delta t_d / \Delta t_0 = \Delta v_0 / \Delta v_d$. In our case, the time magnification is $M \approx 2$.

pulse remains constant[1]—no "brightening" of the focus occurs due to the time-dependent magnetic field [22]. Hence, a simple estimate for the time magnification M can be obtained, where M is defined as the ratio $\Delta t_d / \Delta t_0$ of pulse widths at $t = t_d$ and $t = 0$:

$$M = \Delta t_d / \Delta t_0 \approx \Delta z_d / \Delta z_0 = (t_1 - t_i)/(t_f - t_1). \tag{7}$$

We now derive the magnetic field in the interval between t_i and t_f. The coordinate of a neutron at time t_f is given by

$$z_f = v_0 t_f + a(t_f - t_i)^2 / 2. \tag{8}$$

By substituting Eqs. (2) and (8) into Eq. (3) we get a relation between a and v_0:

$$a = \frac{z_d - v_0 t_d - a(t_f - t_i)^2 / 2}{(t_f - t_i)(t_d - t_f)}, \tag{9}$$

which can be rewritten as

$$a(v_0) = \frac{2(z_d - v_0 t_d)}{(t_f - t_i)(2t_d - t_f - t_i)} = \frac{\bar{v} - v_0}{t_1 - t_i} \tag{10}$$

where $\bar{v} = z_d / t_d$ is the central velocity of the neutrons, which is not affected by the lens action [$a(\bar{v}) = 0$]. Equation (10) determines the acceleration as a function of the initial velocity v_0 of neutrons, it can easily be verified by looking at Fig. 3. With this acceleration each neutron will come to the point z_d at time t_d. To find this acceleration as a function of time and coordinate $a(t,z)$ we need to use the relation between the initial velocity of a neutron, its coordinate, and time. In the interval $t \in [t_i, t_f]$ this relation is

$$z(t) = v_0 t + a(t - t_i)^2 / 2. \tag{11}$$

Substituting it into Eq. (10) we obtain a linear equation in a:

$$a = \frac{\bar{v} - [z(t) - a(t - t_i)^2 / 2]/t}{(t_1 - t_i)}$$

and solving for $a(t,z)$ we get

$$a(t,z) = \frac{2(\bar{v}t - z)}{t_1^2 - t_i^2 - (t - t_1)^2}. \tag{12}$$

The required external force is given by $F(t,z) = m_n a(t,z)$. If this force is due to the gradient of the magnetic field which acts on spins of polarized neutrons, the required magnetic field as a function of (z,t) is determined by

$$\mu_n \frac{\partial B}{\partial z} = -m_n a(t,z), \tag{13}$$

where μ_n is the magnetic moment of the neutron. Writing this relation we assumed that the time derivative of the magnetic field is negligible compared to its space derivative:

---

[1]Generally, the Liouville theorem does not hold for time-dependent Hamiltonians. Luckily, for our special solution (constant acceleration along a particle trajectory with the parabolic potential) the theorem does work (see also our numerical results collected in Sec. IV).

$$\left|\frac{\partial B(t,z)}{\partial z}\right| \gg \frac{1}{c}\left|\frac{\partial B(t,z)}{\partial t}\right|,$$

where c is the light velocity. After integration of Eq. (12) over z we obtain

$$B(t,z) = \frac{m_n}{\mu_n}\frac{(z-\bar{v}t)^2}{t_1^2 - t_i^2 - (t-t_1)^2}. \tag{14}$$

This magnetic field profile is just a parabola widening and shrinking in time and moving with the central velocity $\bar{v}$ of neutrons. The curvature of the parabola changes with time as determined by the denominator in formula (14).

The sign of the field is spin dependent, so that the desired focusing effect will occur for neutrons with one of the two polarizations, which is also significant for aberrations as we briefly discuss below.

The condition of constant acceleration for each neutron implies that each one remains at a position of constant slope of the parabola, and the spatial extension of the neutron pulse in the z direction is equal to the width at maximal slope of the parabola, necessary to focus the initial velocity band Δv_0. The maximal width of the parabola is reached at $t=t_1$ [the denominator of Eq. (14) is maximal there]. At this time the spread of the beam is maximal too and all neutrons are at rest at t_1 in the frame moving with $\bar{v}$ (see also Fig. 3).

In the moving frame ($\bar{v}$) we calculate the width $w(\Delta v)$ of the magnetic bowl. With $v_0 = \bar{v} + \Delta v_0$ we get from Eq. (10)

$$a(\Delta v_0) = -\frac{\Delta v_0}{t_1 - t_i}, \tag{15}$$

which we set equal to Eq. (12) with $z = \bar{v}t + w$, leading to

$$2w(t) = \Delta v_0 \frac{t_1^2 - t_i^2 - (t-t_1)^2}{(t_1 - t_i)}. \tag{16}$$

Replacing z by w in Eq. (14) we get for the B-field in the moving frame:

$$B(t,\Delta v_0) = \frac{m_n}{\mu_n}\frac{\Delta v_0^2}{4}\frac{t_1^2 - t_i^2 - (t-t_1)^2}{(t_1 - t_i)^2}. \tag{17}$$

The condition of constant acceleration, assumed at the beginning, is not mandatory to achieve focusing in time. A nonlinear velocity curve as shown in Fig. 5 can be used as well, as long as Eq. (4) is satisfied. In this case the maximum field strength may be significantly reduced, as the acceleration at t_1, where w is maximum, is lower now. However, in this case the field rise and drop near t_0 and t_f gets faster, and the adiabaticity condition (the neutrons must smoothly turn to the direction of the B field) may be more difficult to satisfy. So it may turn out that low maximal fields at t_0 and t_f are more favorable. These questions request numerical evaluation, which have not yet been done.

Aberrations of magnetic time lenses may arise from field gradients in directions lateral to the optical axis. They may be analyzed in the moving frame, considering $B(t,z)$ as a slowly varying function with respect to t.
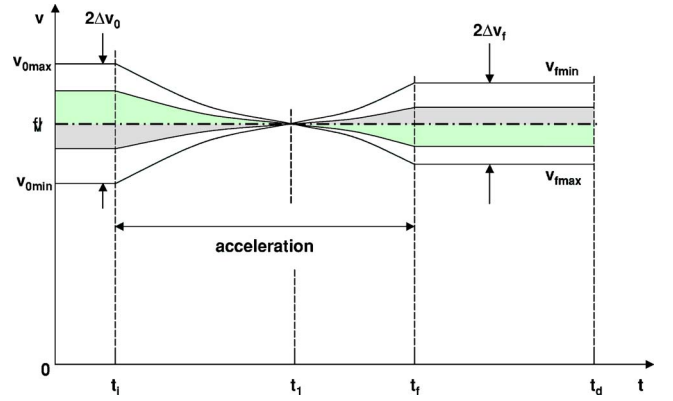

FIG. 5. (Color online) Velocity-time diagram of a time lens with varying acceleration. In this case the maximum field at t_1 is reduced compared to the case of constant acceleration. As before the shaded areas left and right from the principal time t_1 must be equal.

Near the optical axis, from $\nabla \cdot B = 0$ and axial symmetry with $\partial B_x/\partial x = \partial B_y/\partial y$ we get $\partial B_z/\partial z = -2\partial B_x/\partial x$, leading to lateral accelerations a_x, a_y which, according to Eq. (15), are given by

$$a_x(\Delta v_0) = a_y(\Delta v_0) = \frac{\Delta v_0}{2(t_1 - t_i)}.$$

The characteristic dimensions of the beam cross section, defined by neutron guides, will be very small compared to the length of the time lens and consequently the path lengths for acceleration in the lateral direction are very small. For reasonable parameters, the mean change in the lateral velocities v_x, v_y picked up due to lateral accelerations will be in the range of ± 2 m/s (see below). This is still small compared to typical values v_x, v_y determined by the guide properties ($\approx \pm 10$ m/s) and no significant beam widening should occur.

Further aberrations arise for off-axial neutrons, as there the acceleration $a_z(\Delta v_0)$ depends on the distance from the optical axis. Due to the beam divergence of typically 1°, averaging over the different $a_z(\Delta v_0)$ will occur. We analyzed these effects numerically, as they depend in a complex way on the beam geometry and on the shape of the coils which generate the B fields. No serious distortion of the time signal was found.

One more point for the sake of a skeptical reader remains to be clarified. As is well known in classical space optics, it is impossible to obtain a geometrically similar image even for an infinitely small object (except of the trivial case of identical infinite-plane mirror imaging). The fact is a trivial consequence of the longitudinal magnification never equaling the transverse one. However, since our aim is not to have an ideal image of an initial t_i, r_i event but to compress a neutron beam to enhance the intensity for the TOF devices in a certain velocity-time interval, this kind of aberrations, which is a nuisance for space optics, for our aims on the contrary provides valued effects improving TOF time resolution.

There is another cause of aberrations in the standard space optics. It is related to paraxial or Gaussian approximations

which are based on an expansion of phase factors over off-axis distances [23]. Formally we have found the exact space-time trajectory Eqs. (11) and (12), or in other words all aberrations are included (the validity window for the geometrical optics approach is extremely wide since thermal neutron wavelengths are of the order of 1 Å, much smaller than typical sample sizes).

Thus, in principle, in the framework of the special solution of the Newton equations found above, an arbitrarily good resolution can be achieved (except for evident physical and technical constraints that we discuss in the next section). For a more general case (when the condition of constant acceleration for each neutron is not granted), the analytical treatment requires a set of different approximate methods on certain scales of length and time, and one has to consider the aberration problems.

III. DESIGN PARAMETERS AND GAIN FACTORS

For efficient use in a TOF spectrometer, the magnetic lens should be located between the first chopper and the sample (see Fig. 1). The lens region should be as long as possible to keep the maximum field strength B for a given velocity band Δv as low as possible. In TOF spectrometers, in general the distance L_p from the first chopper to the sample is somewhat larger than the distance L_s from the sample to the plane of detection, which helps for choosing a time magnification M close to 1 [see Eq. (7)] with its optimal imaging properties concerning time resolution at the detector.

As design parameters we choose $L_p=14$ m, $L_s=4$ m, and a total length of $L_B=8$ m for the traveling field, starting 5 m behind the first chopper and terminating 1 m before the sample position. As central neutron velocity we take $\bar{v}=600$ m/s, which is a convenient velocity for high-resolution TOF instruments. From these parameters we obtain for the central neutron velocity $t_i=8.3$ ms; $t_f=21.7$ ms; $t_d=30$ ms; $t_1=15$ ms [see Eq. (5)], and $M=1$ [see Eq. (7)].

As minimal opening time $2\Delta t_0$ of the first chopper we take $2\Delta t_0=5$ μs, which is reached by state-of-the-art double-chopper systems for typical beam cross sections of 3 cm width. With $\Delta t_d=M\Delta t_0$, a minimum pulse width at the detector of $2\Delta t_d=5$ μs is achieved. This still matches the time resolution of commonly used gas detector tubes; however, the use of scintillator-based detectors (at least ten times higher resolution) seems preferable in this case.

Equation (17) links the maximal velocity band Δv_0 that can be focused by the time lens to the maximum traveling B field that can be applied. Due to the rather low duty cycle of less than 10% of the field, a maximum field strength of $B=1$ T can be assumed in the following, certainly within reach using state-of-the-art accelerator technologies. From Eq. (17) with $t=t_1$ (where B reaches its maximum value) we get

$$\Delta v_0^2 = 4\frac{B(t_1,\Delta v_0)}{m_n/\mu_n}\frac{t_1-t_i}{t_1+t_i}. \qquad (18)$$

For the above parameters and $m_n/\mu_n=0.173$ kg T/J we get for the velocity band $2\Delta v_0$ to be focused by the time lens

$$2\Delta v_0 = 5.1 \text{ m/s}.$$

Note that this bandwidth depends on the geometry of the spectrometer but to first order it does not depend on the neutron velocity, as the second factor does not depend on v. This favors slow neutrons, as the relative bandwidth increases with wavelength.

A second chopper should be placed at a position $L_1=\bar{v}t_1$; it takes the role of the time aperture for the optics, limiting the velocity band to the nominal width $2\Delta v_0$. Actually it is more convenient to place this chopper after the wanderfeld area with slightly reduced opening time.

For $t_1\gg t_i$, i.e., when the neutrons enter the B field very soon after the first chopper, Eq. (18) gives

$$\frac{1}{4}m_n\Delta v_0^2 = \mu_n B(t_1,\Delta v_0). \qquad (19)$$

This manifests energy conservation in the moving frame, stating that the neutron climbs up the wall of the magnetic bowl, which is very low at t_i and maximal at t_1. The unusual prefactor $1/4$ can easily be understood: in a parabolic bowl, which is constant in time, the force increases linearly with the distance from the center; in our case, however, the force is maximal and constant due to the assumption of constant acceleration. Integrating the force over the distance gives a factor of 2 more in our case compared to the constant bowl.

In the laboratory frame, the energy change ΔE of the neutron is given by

$$\Delta E = mv_0 \Delta v_0$$

which is about two orders of magnitude higher than in the moving frame, as $v_0 \approx 100\Delta v_0$. This demonstrates the high efficiency of the wanderfeld focusing technique.

As usual, there is no unequivocal way to define gain factors. We will compare the present setup with a reference TOF spectrometer, showing the same nominal time resolution of $2\Delta t_d=5$ μs at the detector, based on a geometry that is better adapted for that case: We choose $L_p'=6$ m, $L_s=4$ m, with the second chopper in a distance of 5 m after the first one, i.e., centered between the first chopper and the detector. In this geometry the nominal time resolution of 5 μs is obtained for $2\Delta t_0'=\sqrt{2}\times 5$ μs and $2\Delta t_1'=1/\sqrt{2}\times 5$ μs for the first and second chopper, respectively, neglecting further broadening due to flight path uncertainties. The gain G in intensity by the wanderfeld technique can be estimated by:

$$G = 0.4\frac{\Delta t_0}{\Delta t_0'}\frac{\Delta v_0}{\Delta v_0'} \qquad (20)$$

where $2\Delta v_0'$ is the velocity bandwidth transmitted by the second chopper of the reference spectrometer, when the time opening of the first chopper is infinitely small. The factor 0.4 takes into account the loss in intensity due to beam polarization, necessary for the wanderfeld technique. It includes 20% loss due to nonideal transmission of the polarizer. Polarizations of 98–99 % are easily in reach with state-of-the-art supermirror polarizers or long polarizing guides. For the above parameters we get $2\Delta v_0'=0.26$ m/s and for the gain factor G we get
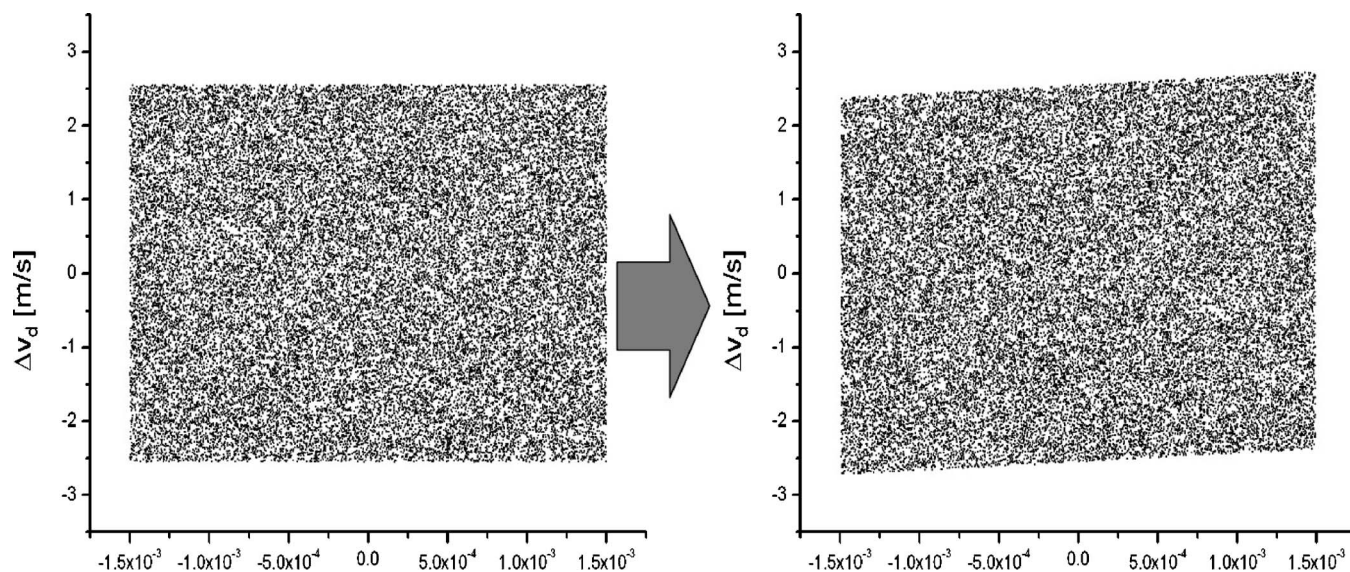
FIG. 6. The evolution of the phase-space element for the ideal time lens with time magnification $M=1$ from the start to the detector, calculated for about 3×10^4 neutrons. The density within the volume remains constant.

$$G = 5.5.$$

This gain is proportional to $\sqrt{B}$, and to $1/\bar{v}$. With more favorable values than taken for the estimate above, gains of one order of magnitude seem within reach. Furthermore the envisaged time resolution of $2\Delta t_d = 5 \ \mu$s at the detector seems not reachable for conventional TOF spectrometers, as a value of $2\Delta t_1' = 1/\sqrt{2} \times 5 \ \mu$s for the opening time of the second chopper cannot be reached with state-of-the-art technology for a neutron beam of reasonable width. We are convinced that the time lens will improve significantly the time resolution in TOF.

IV. NUMERICAL CALCULATIONS

We accompanied the analytic approach by Monte Carlo simulations for (i) the evolution of the phase-space element during propagation through the optical system; (ii) the dependence of the time resolution on the energy transfer at the sample; (iii) the effect of sample size on time resolution; (iv) the optimization of the coil geometry, which generates the traveling field.

The calculations with the ideal parabolic field (Figs. 6 and 7) are done in one space and one time coordinates. For the realistic coil design (Figs. 8–11) a parallel beam of circular cross section with axial symmetry is considered.

If not specified differently, we used the following parameters: mean neutron velocity $\bar{v} = 600$ m/s; mean velocity spread $2\Delta v_0 = 5.1$ m/s; mean chopper opening time $2\Delta t_0 = 5 \ \mu$s; distance from first chopper to sample $L_p = 14$ m; distance from sample to plane of detection $L_s = 4$ m; total length of the traveling field $L_B = 8$ m starting 5 m after the first chopper.

The evolution of the phase space element for the ideal time lens, i.e., for a perfect quadratic potential [Eq. (14)], was already shown in Fig. 4. Using the above parameters, Fig. 6 shows the phase-space volume at the start and at the
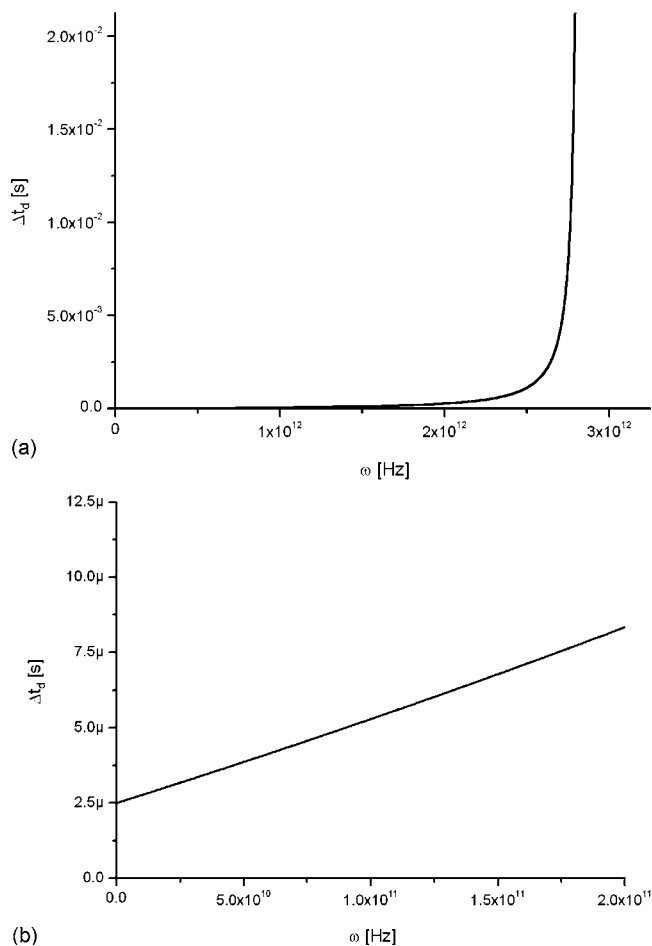

FIG. 7. Evolution of the time resolution Δt_d as function of the energy transfer $\hbar\omega$ upon scattering. The nominal matter-wave energy is $\hbar\omega_0 = 12$ meV (on the right panel the linear part of the time resolution dependence is shown).
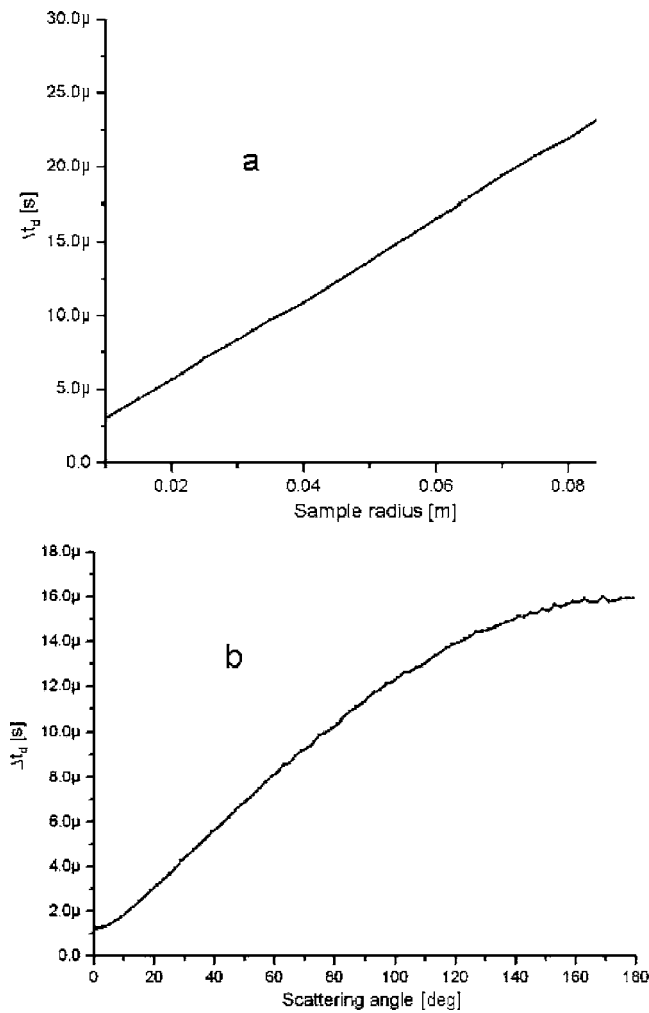
FIG. 8. Effect of sample size and scattering angle on time reso-
lution for a circular sample: the left panel (a) shows that the time
width increases linearly with the radius of the sample for a specific
scattering angle (45° in the figure); the right panel (b) shows the
dependence of the time width on the scattering angle (for 1.5 cm
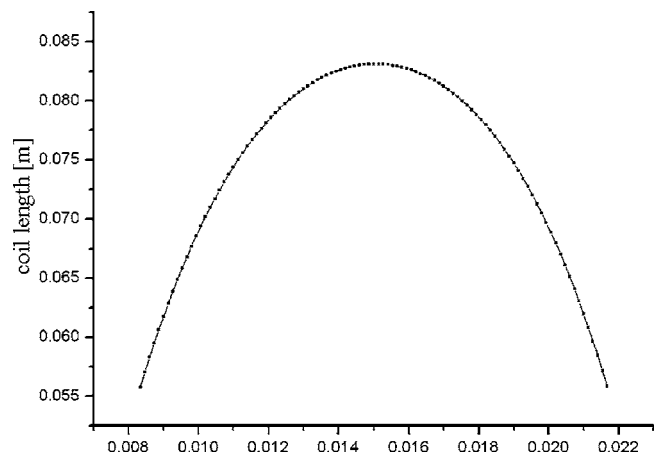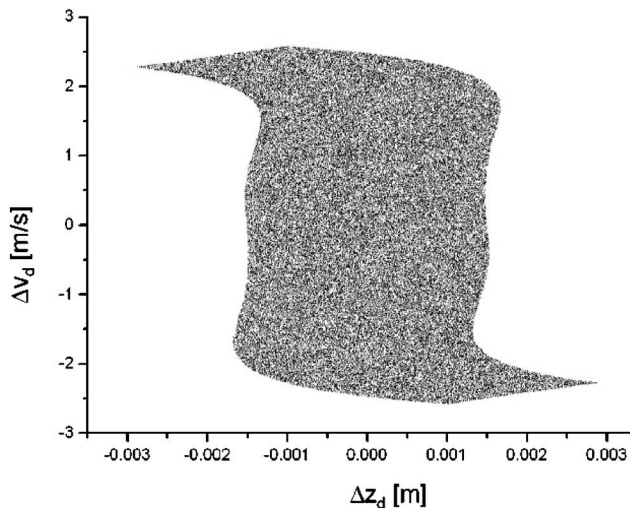sample radius). The fluctuations originate from statistics.

FIG. 9. Variation of coil length from the start time t_i of the time
lens to the end time t_f. Its maximal length is at the principal time t_1,
where the neutron pulse reaches its maximal length. The other pa-
rameters are given in the text.

detector, calculated for about 3×10^4 neutrons; it clearly
demonstrates that the density within the volume remains
constant upon its transform. This also confirms the formula
for time magnification [see Eq. (7)] and apparently Liou-
ville's theorem holds.

As the TOF technique is applied for inelastic scattering,
we checked the influence of energy change $\hbar\omega$ upon sample
scattering on the time resolution of the time optics. Up to ω
values of about 2.0×10^{11} Hz ($\approx 10\%$ of neutron energy), the
time resolution stays below $\Delta t_d = 8$ μs (see Fig. 7). Up to a
$\omega = 2.0 \times 10^{12}$ Hz, corresponding to about 70% of the neutron
energy, and the time widening of the focus goes fairly lin-
early with ω.

Next we examined the effect of sample size and scattering
angle on time resolution, assuming a circular sample and
homogeneous scattering within. The time width increases
linearly with the radius of the sample for a specific scattering
angle as seen on Fig. 8(a). The time width starts to increase
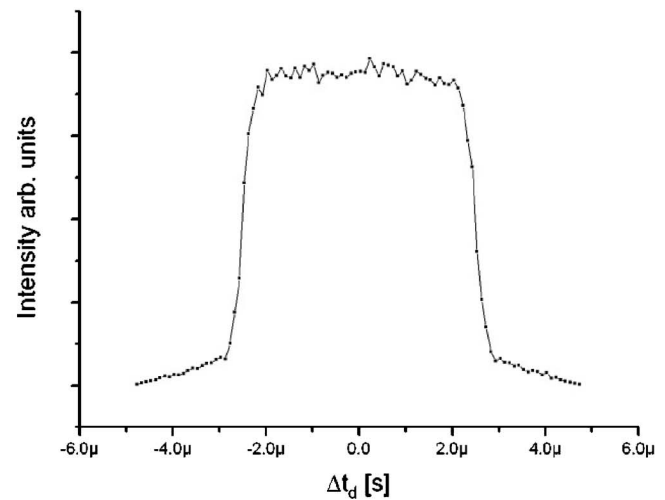quadratically with scattering angle, and finally reaches a

FIG. 10. Phase-space element and time signal at the detector for a realistic setup of coils, generating the traveling field. The "wings" on
both figures are due to a slight deviation from parabolic field shape, experienced by those neutrons, which are at the leading and lagging
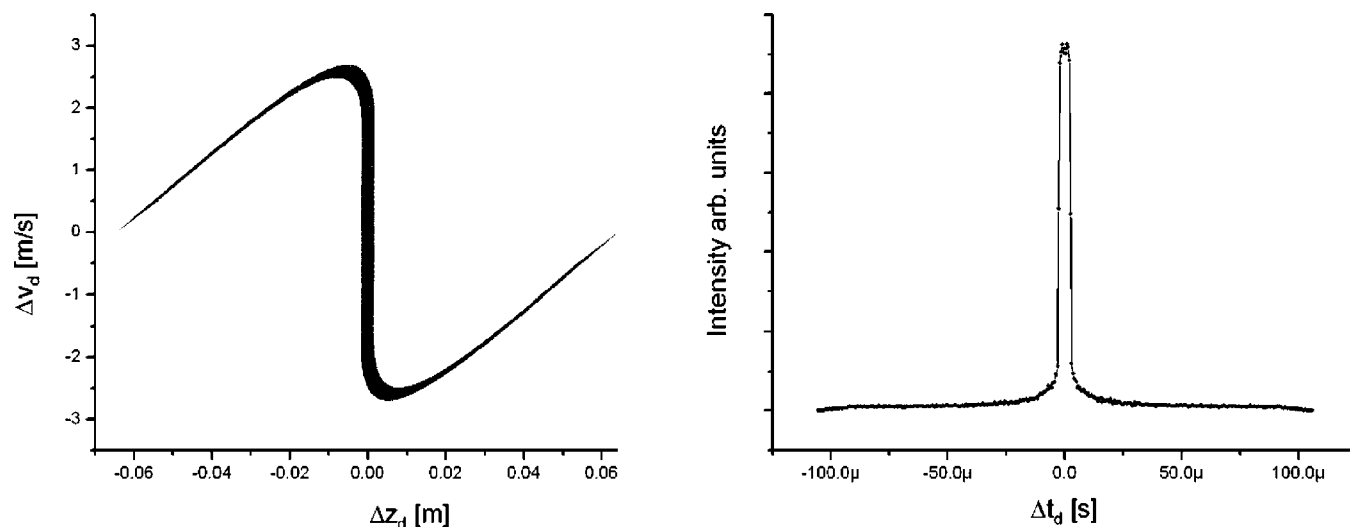edges of the traveling neutron pulse.

FIG. 11. Phase-space element and time signal at the detector for the same traveling field as in Fig. 10, but for a velocity bandwidth nearly twice too large to get properly focused by the lens. The wings seriously distort the time resolution.

maximum of about $\Delta t_d \approx 16~\mu$s at a scattering angle of π for a sample of 1.5 cm radius [Fig. 8(b)].

Next we derived a realistic coil design for a traveling field of near-parabolic shape and calculated for this field the phase-space element at the detector and the corresponding time resolution. A magnetic field of axial geometry with parabolic shape in the z direction implies $\partial B / \partial x = \partial B / \partial y \neq 0$. As discussed earlier, lateral forces proportional to $\partial B / \partial x$ or $\partial B / \partial y$ will not disturb significantly the lens action and therefore were neglected. However, we took into account the reduction of the longitudinal force with the distance from the optical axis, resulting from $\nabla B = 0$.

We assume the field to be realized by a set of cylindrical coils of varying shape and field strength along the z axis. In the calculation we take a coil traveling with $\bar{v}$ with varying radius, length, and current. The following calculations were done for a coil radius of 4 cm, a current of 217 A, 250 turns/cm, and for varying length, as shown in Fig. 9.

Since the duty cycle of the coil is only in the percent-range, the assumed current should be applicable. Figure 10 shows the phase-space element and the time signal at the detector for the setup in mind.

For a bandwidth $\Delta v_0 = 4.4$ m/s (2.5 m/s was used in the example before), the phase-space element and the time distribution show very pronounced tails on both sides, as seen in Fig. 11. Such a broad bandwidth clearly is outside of the focusing capacities of the time lens with the parameters in mind.

We have demonstrated the feasibility of a time lens, which may open further fields for high-resolution neutron TOF instruments. Further calculations will focus on minimizing the tails in the time distribution for larger Δv_0.

ACKNOWLEDGMENT

[1] B. H. Kolner, IEEE J. Quantum Electron. **30**, 1951 (1994).

[2] R. Neutze and G. E. Stedman, Phys. Rev. A **58**, 82 (1998).

[3] M. Arndt, P. Szriftgiser, J. Dalibard, and A. M. Steane, Phys. Rev. A **53**, 3369 (1996).

[4] E. Maréchal, S. Guibal, J.-L. Bossennec, R. Barbé, J.-C. Keller, and O. Gorceix, Phys. Rev. A **59**, 4636 (1999).

[5] S. Bernet, M. K. Oberthaler, R. Abfalterer, J. Schmiedmayer, and A. Zeilinger, Phys. Rev. Lett. **77**, 5160 (1996).

[6] C. W. Roberson and B. Hafizi, Phys. Rev. Lett. **72**, 1654 (1994).

[7] M. Moshinsky, Phys. Rev. **88**, 625 (1952).

[8] A. S. Gerasimov and M. V. Kazarnovskii, Sov. Phys. JETP **44**, 892 (1976).

[9] A. I. Frank and R. Gähler, Phys. At. Nucl. **63**, 545 (2000).

[10] A. I. Frank, P. Geltenbort, G. V. Kulin, and A. N. Strepetov, JETP Lett. **78**, 188 (2003).

[11] A. I. Frank and V. G. Nosov, Phys. At. Nucl. **57**, 968 (1994).

[12] J. Felber, R. Gähler, R. Golub, P. Hank, T. Keller, and U. Rauch, Found. Phys. **29**, 381 (1999).

[13] J. Felber, R. Gähler, C. Rausch, and R. Golub, Phys. Rev. A **53**, 319 (1996).

[14] T. Hils, J. Felber, R. Gähler, W. Gläser, R. Golub, K. Habicht, and P. Wille, Phys. Rev. A **58**, 4784 (1996).

[15] S. V. Grigoriev, W. H. Kraan, and M. Th. Rekveldt, Phys. Rev. A **69**, 043615 (2004).

[16] H. Rauch, in *Neutron Scattering in the Nineties* (IAEA, Vienna, 1985), p. 35.

[17] J. Summhammer, L. Niels, and H. Rauch, Z. Phys. B: Con-

dens. Matter **62**, 269 (1986).

[18] D. Rubio Temprano, K. Conder, A. Furrer, H. Mutka, V. Trounov, and K. A. Müller, Phys. Rev. B **66**, 184506 (2002).

[19] B. Lake, G. Aeppli, T. E. Mason, A. Schröder, D. F. McMorrow, K. Lefmann, M. Isshiki, M. Nohara, H. Takagi, and S. M. Hayden, Nature (London) **400**, 43 (1999).

[20] A. J. Moreno, A. Alegria, J. Colmenero, and B. Frick, Phys.

Rev. B **65**, 134202 (2002).

[21] S. Carretta, E. Liviotti, and G. Amoretti, R. Caciuffo, A. Caneschi, and D. Gatteschi, Phys. Rev. B **65**, 052411 (2002).

[22] W. Ketterle and D. E. Pritschard, Phys. Rev. A **46**, 4051 (1992).

[23] M. Born and E. Wolf, *Principles of Optics*, 4th ed. (Pergamon, Oxford, 1970), Chap. V.